Food Chemistry: X 33 (2026) 103464

Contents lists available at ScienceDirect

Food Chemistry: X

journal homepage: www.sciencedirect.com/journal/food-chemistry-x

Molecular mechanism of synergistic tyrosinase inhibition by blueberry and black chokeberry anthocyanidins: Optimal synergistic formulation for multi-berry beverage development

Yuxin Du [a,1], Lanqiong Zhao [a,1], Zixuan Yuan [a], Yu Zhang [a], Yuxin Chen [a], Yang Ding [a], Xinyao Jiao [a], Chong Zhao [b], Kuniyoshi Shimizu [c], Baoru Yang [d], Zhongxia Li [e], Bin Li [a], Hui Tan [a,*]

[a] College of Food Science, Shenyang Agriculture University, Shenyang, Liaoning 110866, China
[b] College of Food Science and Nutritional Engineering, China Agriculture University, Beijing 100083, China
[c] Department of Agro-Environmental Sciences, Faculty of Agriculture, Kyushu University, 812-8581 Fukuoka, Japan
[d] Food Chemistry and Food Development, Department of Life Technologies, University of Turku, FI-20014 Turun yliopisto, Finland
[e] Nutrition and Health Research Centre, By-Health Co. Ltd, Guangzhou, China

ARTICLE INFO

Keywords:
Tyrosinase
Anthocyanin
Interaction mechanism
Synergistic effect
Food control

ABSTRACT

Tyrosinase is the rate-limiting enzyme in melanogenesis and food browning, making its inhibitors crucial for health and food preservation. However, the specific mechanisms by which multi-berry formulations synergistically inhibit tyrosinase remain uncharacterized, particularly within the context of overcoming bioactivity limitations caused by standardized food ingredients. Our study revealed that blueberry-black chokeberry extracts at 1:1 ratio with superior synergistic inhibition in tyrosinase. Using affinity-ultrafiltration coupled with ultra–performance liquid chromatography–mass spectrometry (AUF–UPLC–MS), sixteen inhibitors were identified, notably delphinidin-3-*O*-galactoside (IC_{50} = 45.06 ± 1.32 μM) and cyanidin-3-*O*-arabinoside (IC_{50} = 55.54 ± 0.83 μM) displayed the highest binding affinities with synergistic inhibition at 4:1-ratio. This anthocyanin mixture exhibited reversible mixed-type inhibition, with Lineweaver-Burk analysis and multi-spectroscopic studies confirming stable complex formation. Molecular docking and dynamics simulations revealed the mixture sequence-specific inhibition mediated by enhanced hydrogen bonding that prevented drastic structural changes. The anthocyanin mixture also exhibited enhanced processing stability. These findings provided mechanistic foundations for developing multi-berry-derived anti-tyrosinase ingredients, enabling bioactivity maximization in industrial food processing.

1. Introduction

Tyrosinase plays a pivotal role as a rate-limiting enzyme in melanogenesis by catalyzing $_L$-tyrosine and $_L$-3,4-dihydroxyphenylalanine ($_L$-DOPA) into their corresponding dopaquinones. These dopaquinones are then further oxidized and polymerized into melanin (Caksa, Baqai, & Aplin, 2022; Molina et al., 2024). Simultaneously, tyrosinase plays a significant role in the enzymatic browning observed in fruits, vegetables, and seafood, dramatically impacting their shelf-life, color, flavor and nutrition values (Muñoz-Pina et al., 2021). Therefore, tyrosinase inhibitors are commonly utilized as food preservatives, which have extensive applications for health promotion and enzymatic anti-browning within the field of food manufacturing and processing industries (Li et al., 2021). Currently, numerous potent tyrosinase inhibitors derived from synthetic and natural resources have been extensively studied, such as 4-hexylresorcinol and kojic acid. However, despite their demonstrated efficacy, safety concerns regarding potential skin irritation, instability, or long-term toxicity have significantly limited their regulatory approval and broad application (Zolghadri et al., 2019).

Berries are natural and nutrient-rich edible sources of bioactive phytochemicals, including phenolic acids, flavonoids, anthocyanins and

* Corresponding author at: Dong ling Road, Shen he District, Shenyang, Liaoning 110866, China.
E-mail address: thth229@syau.edu.cn (H. Tan).
[1] Y. Du and L. Zhao contributed equally to this work as co-first authors.

https://doi.org/10.1016/j.fochx.2025.103464
Received 21 September 2025; Received in revised form 9 December 2025; Accepted 28 December 2025
Available online 8 January 2026

proanthocyanidins, which contribute to their diverse functional properties (Qi et al., 2023; Zhang et al., 2024). Due to their high nutritional value and health-promoting properties, berries are frequently integrated into diverse processed food products- particularly functional beverages- to extend their shelf life and fortify bioactive profiles (Puiggròs et al., 2017). Notably, mixed-fruit beverages incorporating two or more berry varieties have gained significant consumers preference over single-fruit formulations. These blends not only exhibit superior sensory appeal but also demonstrate enhanced nutritional synergy and greater functional benefits compared to their single-fruit counterparts (Theba, Nayi, & Ravani, 2024; Wazed, Sheikh, Akhtaruzzaman, Awal, & Mozumder, 2023). Previous studies have demonstrated that mulberries, particularly extracts derived from purple-colored varieties, exhibited significant tyrosinase inhibition activity (Aramwit, Bang, & Srichana, 2010). Furthermore, synergistic effects have been observed in berries combinations. For instance, the combined administration of raspberries and blackberries has been shown to ameliorate mitigating obesity-induced cardiac inflammation and oxidative stress. Similarly, anthocyanin-rich berry mixtures containing blueberry, bilberry and blackberry demonstrated synergistic activity in suppressing invasive lung cancer cell growth (Kausar et al., 2012; Najjar, Knapp, Wanders, & Feresin, 2022). However, systematic studies investigating the synergistic inhibitory effects of multi-berry combinations on tyrosinase activity remain scarce, and the underlying interaction mechanisms among their bioactive components are still unclear, which hinders the rational design and optimization of highly effective and stable anti-tyrosinase berry formulations.

This study aims to address these challenges by systematically exploring the synergistic anti-tyrosinase potential of berry blends. We hypothesize that specific combinations of key berry-derived inhibitors interact synergistically with tyrosinase, and that this interaction can be optimized and mechanistically decoded (Leporini et al., 2020; Ou, Lin, Zhao, & Xie, 2020). To test this, an integrated analytical strategy—combining affinity-ultrafiltration coupled with UPLC-MS (AUF-UPLC-MS) for ligand fishing, kinetics and fluorescence quenching analyses for interaction profiling, and molecular docking for simulation—was employed. This approach allows us to move beyond empirical blending towards a mechanism-guided design. The findings are expected to elucidate the key inhibitor interactions and their combined mechanism of action, thereby providing a scientific basis for precisely optimizing berry blends. This will facilitate the development of stable, high-efficacy anti-tyrosinase functional ingredients, offering a tangible solution to the limitations imposed by raw material variability.

2. Materials and methods

2.1. Chemicals and reagents

All dry powdered berries were obtained from Dandong Junao Foodstuff Co., Ltd. (Dandong, China). Tyrosinase from mushroom and reaction substrates $_L$-DOPA, and $_L$-tyrosine were purchased from Beijing Solarbio Technology Co., Ltd. (Beijing, China). Cyanidin-3-*O*-arabinoside, cyanidin-3-*O*-galactoside, cyanidin-3-*O*-glucoside, delphinidin-3-*O*-glucoside, delphinidin-3-*O*-arabinoside and delphinidin-3-*O*-galactoside with an HPLC purity >99% were purchased from ChemFaces Biochemical Co., Ltd. (Wuhan, China). Kojic acid (purity >98%) was obtained from Shanghai Yien Chemical Technology Co., Ltd. (Shanghai, China). Microcon ultrafiltration centrifuge tubes (0.5 mL, MWCO 100 kDa) were procured from Millipore Co. Ltd. (Bedford, Massachusetts, USA). Methanol, acetonitrile and formic acid were purchased from Merck Group (Darmstadt, Germany). Sodium dihydrogen phosphate and disodium hydrogen phosphate were obtained from Shanghai Macklin Biotech Co., Ltd. (Shanghai, China). All reagents and chemicals were of analytical grade, and all solutions were prepared with ultrapure water.

2.2. Preparation of berry extracts

The extraction was performed based on our previous method with slight modifications (Tan et al., 2024). Briefly, 20 g of the dried powdered black chokeberry (*Aronia melanocarpa)*, blueberry *(Vaccinium corymbosum)*, blackcurrant (*Ribes nigrum L.*), cranberry (*Vaccinium oxycoccos*), sea buckthorn (*Hippophae rhamnoides*), raspberry (*Rubus corchorifolius*) and strawberry (*Fragaria* × *ananassa Duch*) were mixed with 100 mL of 70% ethanol respectively at a ratio of 1:25 (w/v) for 3 h to obtain the berry extracts. After filtration, the supernatants were decompressed and concentrated to dry at 40 °C by IKA RV 10 digital rotary evaporators (IKA, Staufen im Breisgau, Germany). The resulting berry extracts were obtained after freeze-drying and stored at −80 °C for a maximum of 12 weeks.

2.3. Tyrosinase inhibition assay

The assay was performed according to established methods (Wang, Wang, Xia, Sui, & Si, 2019), employing mushroom tyrosinase as a standard model due to its commercial availability and recognized homology to human tyrosinase. Briefly, $_L$-DOPA (2.5 mM) solution, and different concentrations of sample solutions were sequentially mixed using phosphate-buffered saline (PBS, 0.1 M, pH 6.8) solution in a 96-well plate at 25 °C for 5 min. Tyrosinase solution (1000 U/mL) was then added, followed by incubation for an additional 10 min. Finally, the absorbance of the total solution was measured at 475 nm using a TECAN photometric microplate reader (TECAN, Männedorf, Switzerland). The inhibition rate of tyrosinase activity was calculated by the following formula (1):

$$\text{Inhibition of tyrosinase activity}(\%) = \frac{A_{\text{sample}}}{A_{\text{control}}} \times 100\% \quad (1)$$

where A_{sample} represents the absorbance of the sample; A_{control} represents the absorbance without sample. The IC_{50} values were measured by interpolating the concentration-response curves. Kojic acid (0.03 mg/mL) was used as the positive control.

2.4. Screening and identification tyrosinase inhibitors using AUF–UPLC–quadrupole time-of-flight (Q-TOF)-MS/MS

The screening method has been slightly modified based on previous literature (Hering et al., 2023) and the schematic diagram was depicted in Fig. 2**.** Berry extracts (1.5 mg/mL), $_L$-DOPA (2.5 mM), and tyrosinase (1000 U/mL) were added in a PBS solution (0.1 M, pH 6.8) at 37 °C for 40 min. The reaction solution was transferred to an ultrafiltration centrifuge tube (Microcon 100 kDa; Merck Millipore, MA, USA) and centrifuged 8000 r/min for 30 min to remove non-binding components. An inactivated tyrosinase was subjected to heat treatment in a boiling water bath for 30 min and used as negative control. The experiment involved three groups: (1) the blank group reaction solution without tyrosinase; (2) the sample group with tyrosinase; (3) and the denatured group reaction solution contained inactivated tyrosinase, aiming to eliminate non-specific binding of compounds to enzymes. The binding affinity (AD) between the ligand and tyrosinase was calculated using formula (2):

$$\text{AD}(\%) = \frac{A_1 - A_2}{A_0} \times 100\% \quad (2)$$

where A_1, A_2, and A_0 denote the peak areas of identified compounds in berry extract incubations with inactivated tyrosinase, with and without tyrosinase, respectively.

The non-binding fraction obtained after ultrafiltration reaction mixture was analyzed using UPLC-30AD system (Shimadzu Co., Tokyo, Japan). Separation was performed on a JADE-PAK ODS column (250 mm × 4.6 mm, 5 μm, ECHWAY, China) maintained at 30 °C. The mobile

phase consisted of 8.5% formic acid in water (phase A) and 22.5% acetonitrile, 8.5% formic acid, 22.5% methanol (phase B). The gradient elution was applied at a flow rate of 1.5 mL/min as follows: from 0 to 35 min, the proportion of B changed from 7% to 25%; from 35 to 45 min, its proportion changed from 25% to 65%; from 45 to 46 min, its proportion changed from 65% to 100%. Prior to injection, the extracts were filtered through a 0.22 μm membrane and detection was performed at 535 nm.

Anthocyanin monomer identification was carried out using an Agilent 6530 Q-TOF LC-MS/MS (Agilent Technologies, Santa Clara, California, USA) in a positive ion mode with the following parameters. Chromatographic separation was achieved on an Agilent ZORBAX SB-C18 column (4.6 × 100 mm, 1.8 μm) with an injection volume of 5 mL, maintained at 30 °C; using a mobile phase consisting of 0.1% formic acid in water (A) and acetonitrile (B) at a flow rate of 0.5 mL/min. The gradient program was set as follows: 95–0% A over 0–55 min, followed by isocratic elution at 0% A for 55–60 min. MS analysis was conducted with the following parameters: gas temperature was 360 °C with a flow rate of 7 L/min; the sheath gas temperature was 400 °C with 11 L/min; the input voltage at the outlet of the capillary tube was 150 V; and it was in capillary electrophoresis. The scan range was between 100 and 1000 *m/z*. MS/MS fragmentation data were used to confirm the corresponding peaks of anthocyanin monomers.

2.5. Evaluation of synergy effect in tyrosinase inhibition assay

The tyrosinase inhibition rates of blueberry, black chokeberry or their anthocyanins were investigated in various molar ratio combinations. Initially, multiple concentrations of each extract and compounds were selected to represent the range around the IC_{50} values. Five combination ratios (1,1, 1,4, 4:1, 1:9, and 9:1) of these combinations were diluted into series concentrations and calculated using Chou's median effect equation, and the combination index (CI) values were computed according to a previously published method (Chou, Shapiro, Fu, Chou, & Ulrich-Merzenich, 2019). The synergistic effects of different mixtures were evaluated using CI (CI values >1.1, <0.9 and 0.9–1.1 indicate antagonism effect, synergistic effect, and additive effect, respectively). The CI was calculated for the effective doses at inhibition levels, affected fractions (Fa) of 20, 50, 75% represent the tyrosinase inhibition rate (%) affected by dose of berries at each of the combination ratios. The dose reduction index (DRI) represents the fold-reduction in the dose of each berry extract within a synergistic combination relative to its individual dose at a specific effect level. The CI value and DRI value were calculated by Compusyn software (Combosyn, Inc., Paramus, NJ, USA).

2.6. Kinetics study of tyrosinase inhibition

To assess the reversibility of inhibition against tyrosinase, we maintained a constant $_L$-DOPA concentration (2.5 mM) while systematically varying the tyrosinase concentration (150, 300, 450, 600 U/mL). The reaction velocity (V, ΔOD/min) was determined following the addition of delphinidin-3-*O*-galactoside or cyanidin-3-*O*-arabinoside at concentrations ranging from 0 to 32 μM (0, 4, 8, 16 and 32 μM). To further analyze the type of tyrosinase inhibition, the effect of delphinidin-3-*O*-galactoside, cyanidin-3-*O*-arabinoside and mixture (4:1 ratio) were measured by keeping the tyrosinase concentration (1000 U/mL) and increasing the $_L$-DOPA concentration (0.25, 0.5, 1 and 2 mM). The concentrations of delphinidin-3-*O*-galactoside, cyanidin-3-*O*-arabinoside, and their mixture (4,1 ratio) on tyrosinase activity at varying concentrations: (A) 0, 4, 8, and 16 μM for individual anthocyanins; (B) 0, 5, 25, and 50 μM for the mixed inhibitor system. The Lineweaver–Burk plot was used to determine the tyrosinase inhibition mechanism formulas (3)–(5):

$$\frac{1}{V} = \frac{K_m}{V_{max}}\frac{1}{[S]} + \frac{1}{V_{max}} \quad (3)$$

$$\text{Slope} = \frac{K_m}{V_{max}} + \frac{K_m[I]}{V_{max}K_i} \quad (4)$$

$$\text{intercept} = \frac{1}{V_{max}} + \frac{1}{K_{is}V_{max}}[I] \quad 1(5)$$

where K_i represents the inhibition constant of the inhibitor binding to free enzymes; K_{is} represents the equilibrium constant of the inhibitor binding to the enzyme substrate complex; V and V_{max} are the initial reaction velocity and the maximum initial reaction velocity, respectively; K_m is the Michaelis constant; [I] is the inhibitor concentration and [S] is the substrate concentration.

2.7. Fluorescence spectroscopy analysis

Fluorescence spectroscopy method was used based on previous literature with slight modifications (Zhu et al., 2021). The interaction between tyrosinase solution (2.75×10^{-4} g/L) and different sample solutions concentrations (0, 20, 30, 40 and 50 μM) was measured using an F4600 fluorescence spectrometer (Hitachi, Tokyo, Japan). The samples were measured after 20 min of water bath at 298 K, 318 K, and 338 K, respectively. The slit width was set to 5 nm, the excitation wavelength was 280 nm, and the emission spectrum collection range was 290–320 nm.

2.8. Circular dichroism (CD) spectroscopy

The samples were conducted using a JASCO J-810 spectropolarimeter (JASCO Co., Tokyo, Japan), with scanned in the far ultraviolet region of 200–250 nm at 25 °C and a path length of 1 mm. The proportion of the protein's secondary structure was calculated by Cluster-based Discriminative Neural Networks (CDNN) software (Applied Photo-physics Ltd., Surrey, UK).

2.9. Molecular docking and molecular dynamics simulation

The 3D structure of tyrosinase (PDB: 2Y9X) was retrieved from the RCSB Protein Data Bank (PDB) at the official website (http://www.rcsb.org/). The 3D structures of the ligands (delphinidin-3-*O*-galactoside and cyanidin-3-*O*-arabinoside) were retrieved from the PubChem database. The molecular docking software Discovery studio 2019 was used to predict the possible interaction between the ligands and tyrosinase. Before docking, pretreatments such as water removal, ligand molecular deletion, and hydrogen addition, were performed on the original protein via PyMOL. Tyrosinase Chain A was selected as the acceptor protein. The molecular interaction between the ligands and protein was simulated using the CDOCKER program with 100 running times. Other parameters were set to their default values. Finally, the docking model with the lowest binding energy was analyzed.

Molecular dynamics simulations were conducted with Gromacs v2022.03 using AMBER99SB-ILDN force field. Electrostatic interactions were calculated via Particle-mesh Ewald method, followed by energy minimization using the steepest descent algorithm method. The system was equilibrated for 100 ps in isothermal isovolumetric (NVT) ensemble with V-rescale temperature coupling, followed by 100 ns production run in isothermal isobaric (NPT) ensemble at 300 K and 1 bar. Structural dynamics were evaluated through root mean square deviation (RMSD), RMSF (root mean square fluctuation), radius of gyration (Rg) values, surface area accessible to solution (SASA) and hydrogen bonds analyses. Gibbs free energy was derived from RMSD and Rg values. Binding free energy was calculated using gmx_MMPBSA tool based on the molecular mechanics Poisson-Boltzmann surface area (MMPBSA) method.

2.10. Verification assay

During the verification assay, the samples were divided into six groups: (1) The thermal treatment group involved exposing the sample to different temperatures (25 °C, 50 °C, 75 °C and 100 °C) in the dark for 30 min. (2) The ultrasound treatment group involved subjecting the sample to different ultrasound powers (60, 120, 160 and 240 W) for 10 min at 25 °C while avoiding light. (3) The vitamin C (Vc) or (4) sucrose groups contained various concentrations (2, 4, 6 and 8%*v*/v) of Vc or sucrose solution. (5) The accelerated storage group involved storing the sample in the dark at 25 °C for up to 8 h. (6) Finally, the illumination group involved exposing the sample to a light intensity of 5000 lx (1, 2, 3 and 4 h) using light with LS-4000 UV constant temperature light box (Tianxing Technology Co., Ltd., Beijing, China Co., Ltd.) at 25 °C. A final concentration of 60 μM sample solution was added to each group. The determination of tyrosinase inhibition activity was conducted as described above.

2.11. Statistical analysis

Each experiment was performed at least in triplicate (n = 3–5). Statistical analyses were performed using IBM SPSS Statistics 27 (SPSS Inc., Chicago, IL, USA) and the results were presented as mean ± standard deviation (S.D.). One-way analysis of variance (ANOVA) was used to analyze differences, and a p value of <0.05 was considered a statistically significant difference. Different letters indicated significant differences within groups.

3. Results and discussion

3.1. Tyrosinase inhibition activity and synergistic effects of berries

The inhibition activity of seven berry extracts (black chokeberry, blueberry, blackcurrant, cranberry, sea-buckthorn, raspberry and strawberry) at different concentrations on tyrosinase activity was evaluated. All the tested berry extracts demonstrated inhibitory effects on tyrosinase activity in a dose-dependent manner. Based on the results of the IC_{50} value, the order of the anti-tyrosinase activity of the berry extracts were as follows: black chokeberry > blueberry > blackcurrant > cranberry > sea buckthorn > raspberry > strawberry (Supplemental information Table S1). As shown in Fig. 1A, the IC_{50} values of black chokeberry and blueberry were 0.78 ± 0.69 mg/mL and 0.94 ± 0.69 mg/mL, respectively, indicating the strongest inhibition activity on tyrosinase among all the tested berry extracts. These results were consistent with those of previous studies (Tian et al., 2021) and supported the idea that the tyrosinase inhibition activity of blueberries may mainly depend on the content of anthocyanins. A previous study also showed that the mixture of delphinidin-3-*O*-glucoside and cyanidin-3-*O*-glucoside displayed a more potent anti-inflammatory effect compared with that of a single anthocyanin, suggesting that a combination of diverse anthocyanins might exert synergistic effects (Zhu et al., 2013). Therefore, it is highly speculated that a synergistic effect might exist among the berries.

Five gradient-designed concentration ratio combinations were investigated to further explore whether there was a synergistic effect between blueberry and black chokeberry on tyrosinase inhibition activity. The CI value was employed to quantitatively evaluate the combined effects between two berry extracts. A CI value below 0.9 indicated a synergistic effect, suggesting that the combined extracts exhibited enhanced tyrosinase inhibition compared to individual extracts. As shown in Fig. 1B–C and Table 1, all tested combinations of blueberry and black chokeberry extracts exhibited a synergistic effect. Specifically, synergy was evident at concentration ratio of 9:1 with Fa of 20%; at 1:1 and 4:1 concentration ratio when Fa at 75%. A progressively stronger synergistic effect was observed for the 1:1 blueberry–black chokeberry mixture with increasing Fa levels, ranging from slight to strong synergism. Notably, this ratio demonstrated the lowest CI value (0.46 ± 0.19) at a high Fa of 75% and higher for across all the tested combinations with the DRI values of 5.5 and 3.1 for blueberry and black chokeberry, respectively, which indicated that it was the optimal combination concentration for blueberry and black chokeberry, exerting the most robust synergistic effect on tyrosinase inhibition.

3.2. Screening of tyrosinase inhibitory ligands using AUF–UPLC–Q-TOF-MS/MS

AUF–UPLC–MS/MS is an effective approach for the rapid screening and targeted separation of potential active components in herbal extracts (Li et al., 2022; Liu et al., 2024). Upon incubation, the active ingredients from berry extracts formed a tyrosinase-inhibiting complex. Subsequently, this complex can be segregated from inactive components by exploiting the selective retention property of centrifugal ultrafiltration filters. Finally, twelve and four main anthocyanins were identified using UPLC–Q-TOF-MS/MS in blueberry and black chokeberry extracts respectively. The detail results after comparing chromatographic retention times, excimer ion peak features, MS^2 fragmentation patterns and relevant literature (Gao et al., 2023; Tan et al., 2024; Zang et al., 2021) were presented in Supplemental information Table S2. The chemical structures and their calculated binding levels were shown in Fig. 2A. After comparing the chromatograms of berry extracts that were incubated in the absence of tyrosinase, it was observed that the peak areas corresponding to the compounds that bind to tyrosinase were significantly reduced, indicating that these compounds may interact with tyrosinase through specific or non-specific binding. Non-specific binding can be excluded by comparing with the chromatogram of berry extracts incubated with inactivated tyrosinase. Among the twelve anthocyanins found in blueberry extract, delphinidin-3-*O*-glucoside (12.93% ± 2.14%, peak 2) showed a high level of binding ability, followed by delphinidin-3-*O*-galactoside (10.15% ± 1.52%, peak 1), and delphinidin-3-*O*-arabinoside (9.195 ± 0.73%, peak 4), as calculated

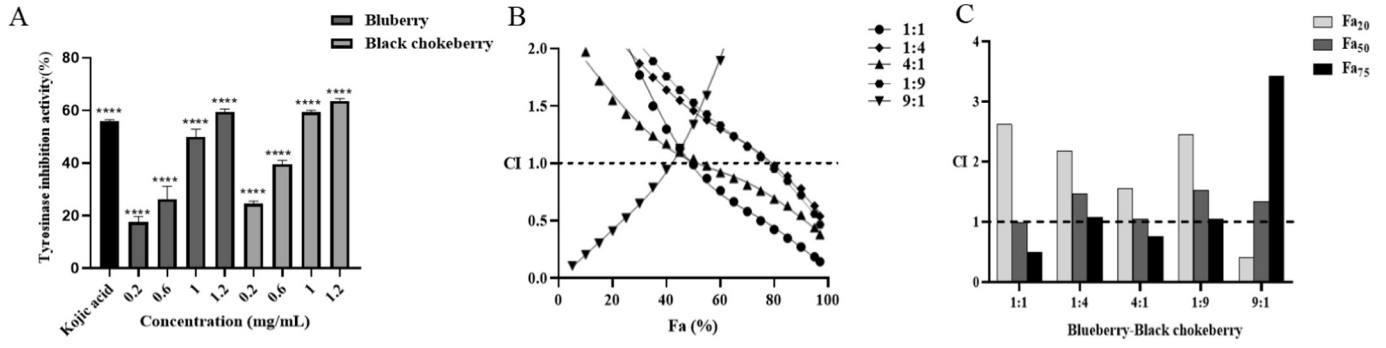

Fig. 1. (A) The tyrosinase inhibitory activity of blueberry and black chokeberry; (B–C) The CI values of blueberry and black chokeberry in different concentration ratio combinations (1,1, 1,4, 4,1, 1,9, 9:1).

Table 1
The CI and DRI values of blueberry and black chokeberry extract at different combination ratios.

Fa (%)	Treatment dose (mg/mL)		Combination		CI	DRI	
	Blueberry	Black chokeberry	Ratio	Dose (mg/mL)		Blueberry	Black chokeberry
20	0.35	0.19	1:1	0.2 + 0.2	2.62 ± 0.14	0.6	1.2
			1:4	0.1 + 0.4	2.18 ± 0.15	3.0	0.5
			4:1	0.4 + 0.1	1.55 ± 0.09	0.9	2.5
			1:9	0.06 + 0.6	2.45 ± 0.21	5.4	0.4
			9:1	0.1 + 0.01	0.41 ± 0.13	2.8	18.5
50	0.94	0.9	1:1	0.5 + 0.5	0.98 ± 0.06	2.0	2.0
			1:4	0.2 + 0.8	1.47 ± 0.30	4.0	0.8
			4:1	0.7 + 0.2	1.04 ± 0.41	1.3	4.1
			1:9	0.1 + 1.0	1.53 ± 0.26	7.9	0.7
			9:1	1.0 + 0.1	1.34 ± 0.12	0.8	6.2
75	2.28	2.08	1:1	1.2 + 1.2	0.46 ± 0.19	5.5	3.1
			1:4	0.3 + 1.3	1.07 ± 0.15	5.2	1.1
			4:1	1.1 + 0.3	0.76 ± 0.24	1.7	6.0
			1:9	0.2 + 1.5	1.05 ± 0.24	10.7	1.0
			9:1	5.4 + 0.6	3.42 ± 0.38	0.3	2.6

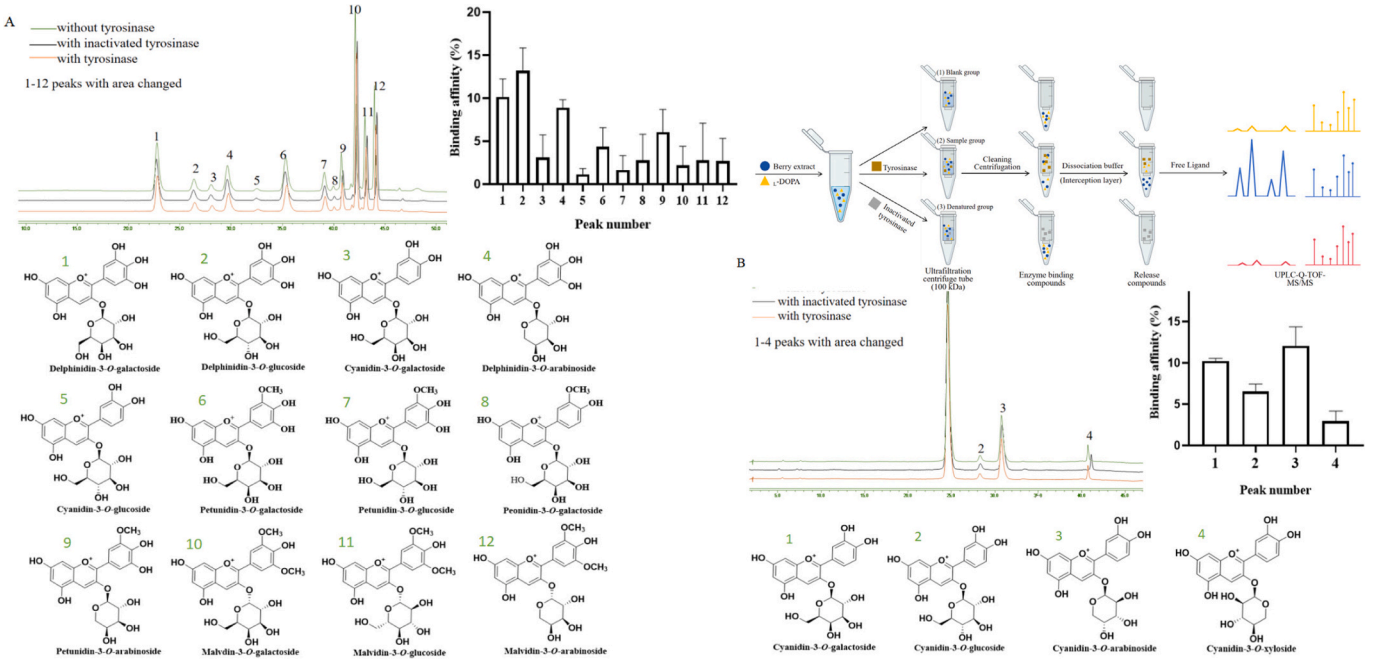

Fig. 2. The schematic diagram of AUF–UPLC–Q-TOF-MS/MS, HPLC chromatogram, chemical structures and corresponding analyses with AD validation against tyrosinase.in blueberry (A) and black chokeberry (B).

using the AD value. As shown in Fig. 2B, among the four anthocyanins found in black chokeberry extracts, cyanidin-3-*O*-arabinoside showed a relatively strong AD value (12.07% ±1.47%, peak 3), followed by cyanidin-3-*O*-galactoside (10.20% ± 0.31%, peak 1), and cyanidin-3-*O*-glucoside (6.52% ± 0.84%, peak 2). These results suggested that anthocyanins could directly interact with tyrosinase. For further validation, anthocyanins with high AD values were selected as key components to analyze their potential on tyrosinase inhibition activity.

3.3. Tyrosinase inhibitory effect and kinetic study of the main active ingredients

Based on the above results, the tyrosinase inhibition activity of six anthocyanins from blueberry and black chokecherry which were identified to have high AD values was further evaluated. As the result shown in Fig. 3A, delphinidin-3-*O*-galactoside and cyanidin-3-*O*-arabinoside from blueberry and black chokeberry exhibited the strongest inhibitory activity against tyrosinase, with the IC_{50} values of 45.06 ± 1.32 μM and 55.54 ± 0.83 μM, respectively. Therefore, their synergistic effect of them was studied in several different concentration ratio combinations. As depicted in Fig. 3B-C and Supplemental information Table S3, the synergistic effect of delphinidin-3-*O*-galactoside and cyanidin-3-*O*-arabinoside at concentration ratio combination of 1:4 and 4:1 increased with an increase in Fa levels. The synergetic effect was observed at Fa of 50% for concentration ratios of 1:4 and 4:1, respectively. Moreover, 4:1 was the optimal combination concentration ratio for tyrosinase inhibition with the lowest CI value (0.62 ± 0.15) at a high Fa of 75%. The DRI values were determined to be 5.9 and 2.2, respectively.

The inhibition mechanism of delphinidin-3-*O*-galactoside, cyanidin-3-*O*-arabinoside and their mixture at a combination ratio of 4:1 was further investigated. As shown in Fig. 3D–E, increasing the concentration of delphinidin-3-*O*-galactoside and cyanidin-3-*O*-arabinoside

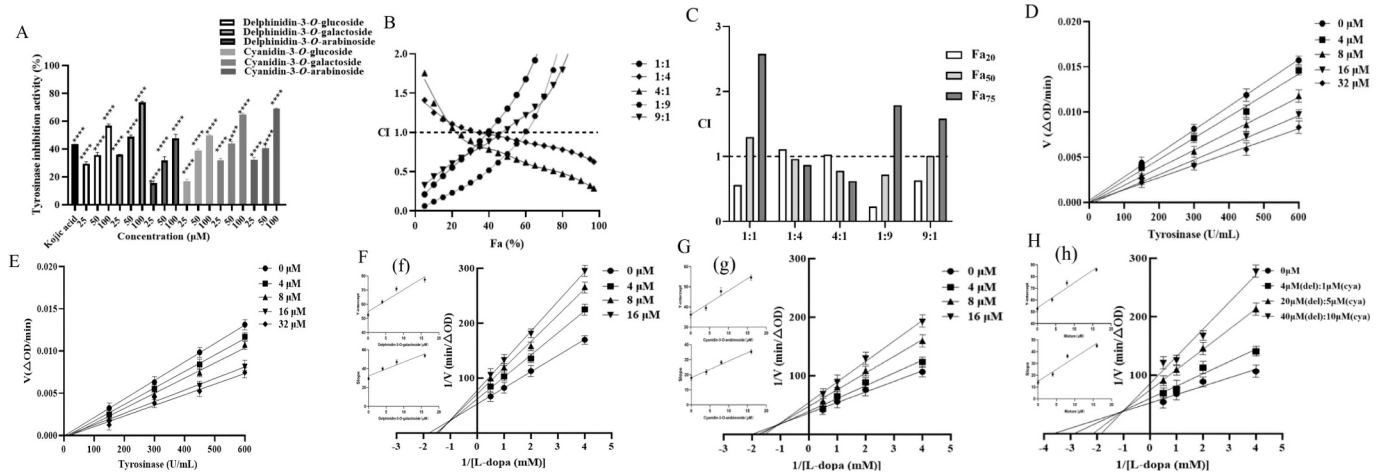

Fig. 3. (A) Analysis of the tyrosinase inhibitory activity of the main active ingredients in blueberry and black chokeberry; (B–C) The CI values of delphinidin-3-*O*-galactoside and cyanidin-3-*O*-arabinoside in different concentration ratio combinations (1:1, 1:4, 4:1, 1:9 and 9:1). (D-E) The relationship between the concentration of tyrosinase and V of delphinidin-3-*O*-galactoside and cyanidin-3-*O*-arabinoside at different concentrations (0, 4, 8, 16, 32 μM). (F–H) Lineweaver-Burk curve of the inhibitory effect of delphinidin-3-*O*-galactoside, cyanidin-3-*O*-arabinoside and mixture (4:1 ratio) on tyrosinase inhibition activity at different concentrations (0, 4, 8, 16 μM for individual anthocyanins and 0, 5, 25, 50 μM for the mixed inhibitor system); (f–h) The second plots (the upper left) represent the intercept and slope of Lineweaver-Burk plot versus delphinidin-3-*O*-galactoside, cyanidin-3-*O*-arabinoside and mixture (4:1 ratio) in the inset.

reduced the tyrosinase activity. All lines passed through the origin with a good linearity, and the slope was negatively correlated with the concentrations, indicating that delphinidin-3-*O*-galactoside and cyanidin-3-*O*-arabinoside demonstrated a reversible inhibitory effect on tyrosinase. The type of tyrosinase inhibition was further investigated using Lineweaver–Burk plots as shown in Fig. 3F–H and Supplemental information Table S4. As the concentrations of delphinidin-3-*O*-galactoside, cyanidin-3-*O*-arabinoside, and their mixture (4:1 ratio) increased, the V_{max} value decreased while the K_m value increased. All fitting lines with different slopes intersected in the second quadrant of the coordinate axis, indicating that they were all mixed-type of inhibitors against tyrosinase (Copeland, 2013; Song et al., 2021). Meanwhile, the smaller K_i value of the mixture (4:1 ratio) indicated its stronger binding ability with tyrosinase. The K_i value of the mixture (4,1 ratio, 7.50 ± 0.86 μM) was much smaller than that of delphinidin-3-*O*-galactoside (22.44 ± 1.07 μM) and cyanidin-3-*O*-arabinoside (16.10 ± 0.48 μM) individually, suggesting that the mixture (4:1 ratio) showed the better inhibition effect on tyrosinase than single, which was consistent with our previous

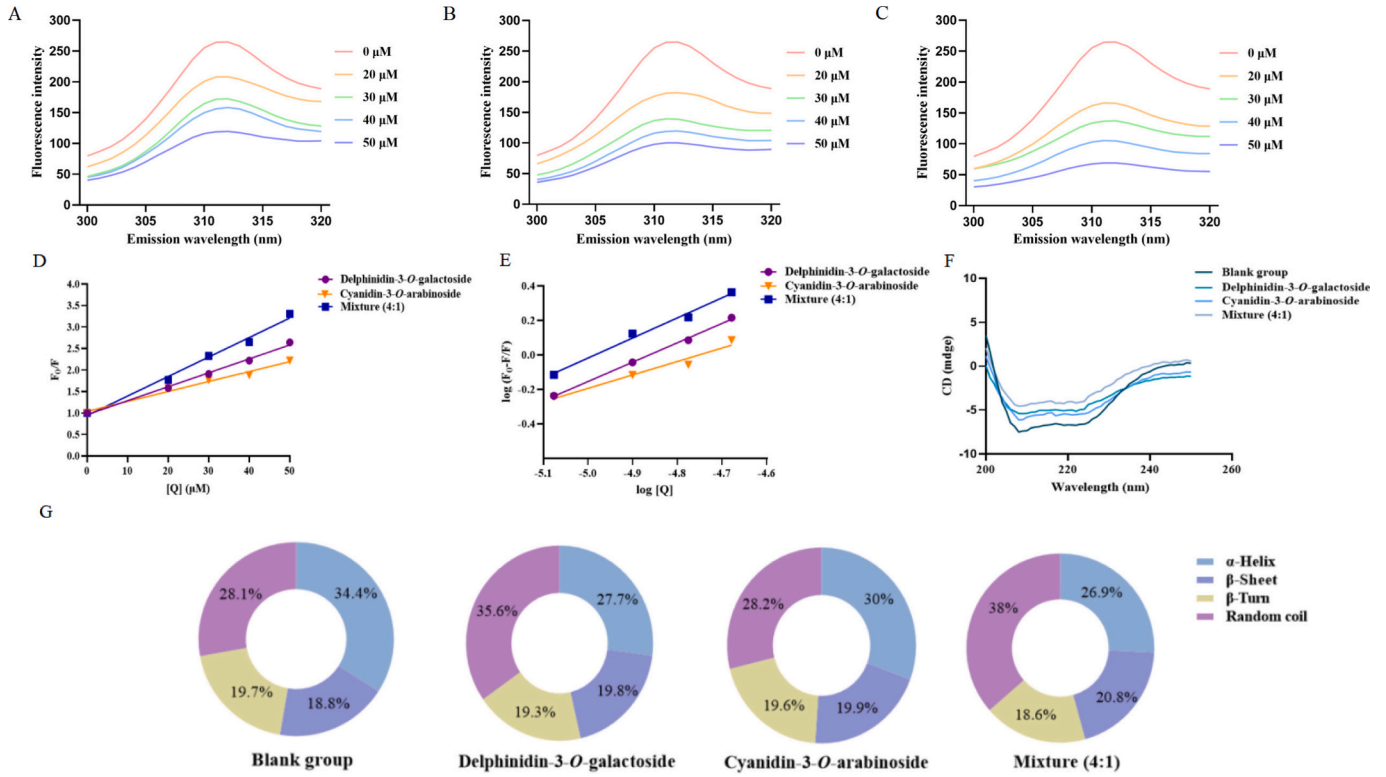

Fig. 4. (A–C) Effect of compounds on the fluorescence spectra of tyrosinase in presence of 0–50 μM each sample, delphinidin-3-*O*-galactoside (A), cyanidin-3-*O*-arabinoside (B), their mixture (4:1 ratio, C) at 298 K; (D–E) Stern-Volmer plots and double-logarithmic regression plots of each compound; (F–H) Effect of compounds on secondary structure content of tyrosinase analyzed by CD spectra.

results. The constants K_i values of mixture (4,1 ratio) were calculated to be lower than the K_{is} value (25.34 ± 2.52 μM), indicating that its affinity with free enzymes is greater than that with the enzyme-substrate complex (Cardullo et al., 2020; Zhao, Wen, Lu, & Liu, 2020).

3.4. Analysis of the quenching mechanism by fluorescent spectroscopy

Fluorescence spectroscopy was employed to further explore the interaction mechanisms between delphinidin-3-*O*-galactoside, cyanidin-3-*O*-arabinoside and their mixture (4:1 ratio) with tyrosinase. As shown in Fig. 4A–C, the addition of each sample dose-dependently decreased the fluorescence intensity of tyrosinase, indicating that delphinidin-3-*O*-galactoside, cyanidin-3-*O*-arabinoside and their mixture (4:1 ratio) interacted with tyrosinase. No obvious shift in the maximum fluorescence absorption peak of tyrosinase was observed as the concentration of cyanidin-3-*O*-arabinoside and delphinidin-3-*O*-galactoside increased. With the addition of their mixture (4:1 ratio), the maximum fluorescence absorption peak of tyrosinase showed a slightly blue shift, and the maximum emission wavelength shifted from 312.2 nm to 311.2 nm, indicating that the mixture (4,1 ratio) altered the conformational environment of the intrinsic fluorescence chromophore.

The Stern–Volmer plots of the delphinidin-3-*O*-galactoside, cyanidin-3-*O*-arabinoside and their mixture (4:1 ratio) tyrosinase reaction system showed a good linear relationship under the temperature of 298 K, implying that only one quenching mechanism is involved in this reaction system (Fig. 4D). The quenching parameters were presented in Table 2. At temperatures of 298 K, 318 K and 338 K, the quenching constant (K_{sv}) was negatively correlated with temperature. The quenching rate constant (K_q) values ranged from 16.6 to 45.4 × 10^{11} L·mol^{-1}·s^{-1}, which was significantly higher than the limit quenching constant of diffusion collision (2.0 × 10^{10} L•mol•s^{-1}), indicating that the binding was a static quenching process. At each of these temperatures (298 K, 318 K and 338 K), the K_{sv} value of the mixture (4:1 ratio) was considerably higher than those of delphinidin-3-*O*-galactoside and cyanidin-3-*O*-arabinoside individually, implying that the mixture exhibited a more potent intrinsic fluorescence quenching effect on tyrosinase than that of a single anthocyanin. This could be due to the synergistic interaction between the components of the mixture, leading to a more stable complex formation with tyrosinase and a greater reduction in fluorescence intensity. Meanwhile, the values of binding constant (K_a) and number of binding sites (n) obtained from the intercept and slope were presented in Fig. 4E and Table 2. At temperatures of 298 K, 318 K and 338 K, the K_a value decreased as temperature increased, indicating that these reactions were spontaneous exothermic processes. An n value of 1 implied that there is only one binding site between ligands and tyrosinase. At each tested temperature, the mixture (4:1 ratio) consistently displayed the highest K_a value (26.46 ± 0.04 at 298 K, 24.43 ± 0.03 at 318 K and 17.36 ± 0.05 at 338 K) compared to individual anthocyanins, indicating its superior binding affinity for tyrosinase.

The thermodynamic constants of enthalpy change (Δ*H*), entropy change (Δ*S*), and Gibbs free energy change (Δ*G*), which play a crucial role in determining the interaction mode of the binding force, were presented in Table 2. The negative Δ*H*, Δ*S* values for delphinidin-3-*O*-galactoside, cyanidin-3-*O*-arabinoside and their mixture (4:1 ratio) provided evidence that the main interaction forces with tyrosinase were hydrogen bonding and van der Waals forces. The negative value of Δ*G* indicated that the reaction was spontaneous. This analysis helped to understand the nature of the interaction between the anthocyanin mixture and tyrosinase and provided insights into the thermodynamic factors that drive the binding.

3.5. Interaction mechanism by CD spectroscopy

CD spectroscopy is widely employed to study the alteration change in structure and conformation of protein when they interact with small molecules (Zhang et al., 2023). As shown in Fig. 4F–G, a significant alteration in the secondary structure content of tyrosinase were observed upon the addition of delphinidin-3-*O*-galactoside/cyanidin-3-*O*-arabinoside and their mixture (4:1 ratio), the contents of the *α*-helix, *β*-sheet, *β*-turn, and random coil structures in the protein were calculated. CD spectra revealed two primary negative bands in the UV region at approximately 209 nm and 222 nm. While minor wavelength shifts occurred among delphinidin-3-*O*-galactoside, cyanidin-3-*O*-arabinoside and their mixture (4:1 ratio). Compared with the blank group, the percentage *α*-helix and *β*-turn in content of tyrosinase decreased, this reduction was notably more substantial when their mixture (4:1 ratio) was added. For instance, after the addition of delphinidin-3-*O*-galactoside, cyanidin-3-*O*-arabinoside, and the mixture (4:1 ratio), the *α*- helix content decreased from 34.4% to 27.7%, 30.0% and 26.9% respectively. The *β*-turn content decreased from 19.7% to 19.3%, 19.6% and 18.6%, respectively. In contrast, the *β*-sheet and random coil content increased, especially when the mixture (4:1 ratio) was added. Specifically, the *β*-Sheet content increased from 18.8% to 19.8%, 19.9% and 20.8% and the random coil content increased from 28.1% to 35.6%, 28.2% and 38% after addition of delphinidin-3-*O*-galactoside, cyanidin-3-*O*-

Table 2
The binding and thermodynamic parameters of compounds with tyrosinase at different temperatures.

Reaction system	*T* (K)	K_{sv} (×10^3 L mol^{-1})	K_q (×10^{11} L mol^{-1} s^{-1})	R^2	K_a (×10^4 L mol^{-1})	n	R^2	Δ*H* (kJ mol^{-1})	Δ*S* (J mol^{-1} k^{-1})	Δ*G* (kJ mol^{-1})
Delphinidin-3-*O*-galactoside	298	32.4 ± 0.12^{c}	32.4 ± 0.12^{c}	0.9944	17.48 ± 0.01^{c}	1.1228	0.9977	−125.63 ± 1.67^{b}	−296.87 ± 1.57^{b}	−31.23 ± 0.02^{f}
	318	27.6 ± 0.07^{e}	27.6 ± 0.07^{e}	0.9844	15.18 ± 0.02^{e}	1.2613	0.9969			−31.14 ± 0.04^{e}
	338	24.4 ± 0.04^{f}	24.4 ± 0.04^{f}	0.9896	12.83 ± 0.03^{f}	1.3550	0.9943			−30.78 ± 0.01^{d}
Cyanidin-3-*O*-arabinoside	298	28.2 ± 0.11^{e}	28.2 ± 0.11^{e}	0.9821	11.65 ± 0.04^{g}	0.7790	0.9930	−78.25 ± 0.24^{a}	−173.99 ± 0.78^{a}	−26.41 ± 0.06^{b}
	318	23.5 ± 0.08^{f}	23.5 ± 0.08^{f}	0.9935	9.89 ± 0.01^{h}	0.8388	0.9843			−22.10 ± 0.02^{a}
	338	16.6 ± 0.06^{g}	16.6 ± 0.06^{g}	0.9812	6.12 ± 0.02i	0.8053	0.9980			−36.69 ± 0.02^{i}
Mixture (4:1)	298	45.4 ± 0.04^{a}	45.4 ± 0.04^{a}	0.9898	26.46 ± 0.04^{a}	1.1640	0.9883	−165.61 ± 0.66^{c}	−381.43 ± 0.57^{c}	−35.24 ± 0.05^{b}
	318	37.2 ± 0.08^{b}	37.2 ± 0.08^{b}	0.9885	24.43 ± 0.03^{b}	1.3730	0.9898			−34.83 ± 0.03^{g}
	338	30.1 ± 0.05^{d}	30.1 ± 0.05^{d}	0.9813	17.36 ± 0.05^{d}	1.4149	0.9967			

arabinoside and their mixture (4:1 ratio), respectively. These results demonstrated that the anthocyanin mixture exerted a more significant impact on the secondary structure compared with the individual components. The alteration within the secondary structure led to the disruption of the enzyme's conformation and its original hydrogen bond network. Such disturbance brought about a change in the enzyme's hydrophobicity, eventually resulting in a breakdown of the enzyme conformation and a consequent reduction in its activity (Song et al., 2020). These results were consistent with the fluorescence spectral data mentioned earlier.

3.6. Molecular docking analysis

Molecular docking is a valuable tool for predicting the binding sites, key residues, and binding forces between receptors and ligands (Xue et al., 2022). As shown in Fig. 5A–C, the predicted optimal binding modes for delphinidin-3-*O*-galactoside, cyanidin-3-*O*-arabinose, and their mixture (4:1 ratio) were molecularly docked with tyrosinase with binding energies of −6.0846, −5.4767 and −6.2279 kcal/mol, respectively. It is evident that the mixture complexes and tyrosinase have the lowest strength of bonding ability, indicating the binding force of the mixture was stronger compared with that of the individual compounds. The results were also in agreement with the IC_{50} value, kinetics and fluorescence quenching results.

As presented in Table 3, molecular interaction analysis between tyrosinase and delphinidin-3-*O*-galactoside (TYR-D3G) revealed that a total of two hydrogen bonds (green dotted line) were formed between delphinidin-3-*O*-galactoside and residues at Glu322 (1.93 Å) and Asn260 (1.71 Å). Four residues, Val283 (2.90 Å), His85 (4.12 Å), His244 (5.39 Å) and His263 (5.57 Å), were involved in the formation of hydrophobic interactions (pink dotted line). Asp312 residues on tyrosinase formed electrostatic interactions (orange dotted line) with the oxygen atom of the C ring with a distance of 3.4 Å. Accordingly, molecular interaction analysis between tyrosinase and cyanidin-3-*O*-arabinoside (TYR-C3A) revealed that residues Asn260 (2.85 Å) and Glu322 (1.99 Å) formed two hydrogen bonds with the hydroxyl group at position 5 of the A ring and position 4′ of the B ring of cyanidin-3-*O*-arabinoside. Residues Val248 (5.42 Å) and Val283 (4.86 and 4.50 Å) were involved in the formation of hydrophobic interactions. Glu256 was involved in an electrostatic interaction with the oxygen atom of the C ring with 4.78 Å. The active site of the tyrosinase contains two copper ions coordinated each by three highly conserved histidine residues, including His 263, His 296, His259, His 61, His 85 and His94 (Decker & Tuczek, 2017). It was worth noting that delphinidin-3-*O*-galactoside interacted with two copper ions and two conserved histidine residues in the active site, explaining its superior inhibitory activity.

The combination of delphinidin-3-*O*-galactoside and cyanidin-3-*O*-arabinoside was studied to understand their binding pattern and ensure that the first docking would have no impact on the structure of tyrosinase (Supplemental information Fig. S1–2). Two distinct docking sequences were analyzed: (1) tyrosinase first with cyanidin-3-*O*-arabinoside followed by delphinidin-3-*O*-galactoside (TYR-C3A-D3G complex), and (2) tyrosinase first with delphinidin-3-*O*-galactoside followed by cyanidin-3-*O*-arabinoside (TYR-D3G-C3A complex). In the TYR-C3A-D3G complex, molecular interaction analysis revealed cyanidin-3-*O*-arabinoside formed three hydrogen bonds with Asn260 (1.98 Å and 1.96 Å), and Glu322 (1.96 Å). Meanwhile, delphinidin-3-*O*-galactoside formed eight hydrogen bonds with key residues in the binding pocket: His85 (1.81 Å and 2.04 Å), Glu322 (1.86 Å), Asn320 (1.80 Å), Val88 (1.82 Å), Met319 (2.41 Å), Glu239 (1.98 Å) and Arg321 (2.20 Å). An additional hydrogen bond was observed between delphinidin-3-*O*-galactoside and cyanidin-3-*O*-arabinoside. Molecular interaction analysis of the TYR-D3G-C3G complex revealed delphinidin-3-*O*-galactoside formed two hydrogen bonds with Glu322 (3.68 Å), Asn260 (2.92 Å). Cyanidin-3-*O*-arabinoside formed six hydrogen bonds with Asn243 (3.76 Å), Met319 (3.88 Å), Asn320 (3.90 Å), Arg321 (3.76 Å), and Glu322 (3.75 Å and 4.42 Å).

Our results demonstrated that the number and strength of hydrogen bonds critically influence binding efficacy. The TYR-C3A-D3G complex, with its extensive hydrogen-bonding network, promoted superior tyrosinase inhibition by preferentially occupying key residues (e.g., His85) and inducing conformational adjustments in the active site. Conversely, TYR-D3G-C3A complex exhibited reduced synergy, likely due to competitive binding at overlapping sites, and weaker intermolecular stabilization between delphinidin-3-*O*-galactoside and cyanidin-3-*O*-arabinoside. Unlike previous studies (Abdurrahim, Temelli, Mazurak, Benruwin, & Chen, 2021), we revealed that the synergistic effect is not simply additive but is highly dependent on the sequence in which components access the active site. This study highlighted the importance of docking order in multi-ligand systems, where sequential binding can either enhance or diminish synergistic effects through residue-specific interactions and conformational modulation.

3.7. Molecular dynamics simulation

Molecular docking has constraints in fully elucidating the impact of ligands on proteins. Conversely, molecular dynamics simulation enables continuous observation of binding stability and dynamic interactions of ligands-protein complexes (Xue et al., 2022). We conducted 100 ns molecular dynamics simulations revealed the TYR-C3A-D3G complex as exhibiting superior structural stability. RMSD is an important basis to evaluate the conformation stability of systems. As shown in Fig. 6A–E,

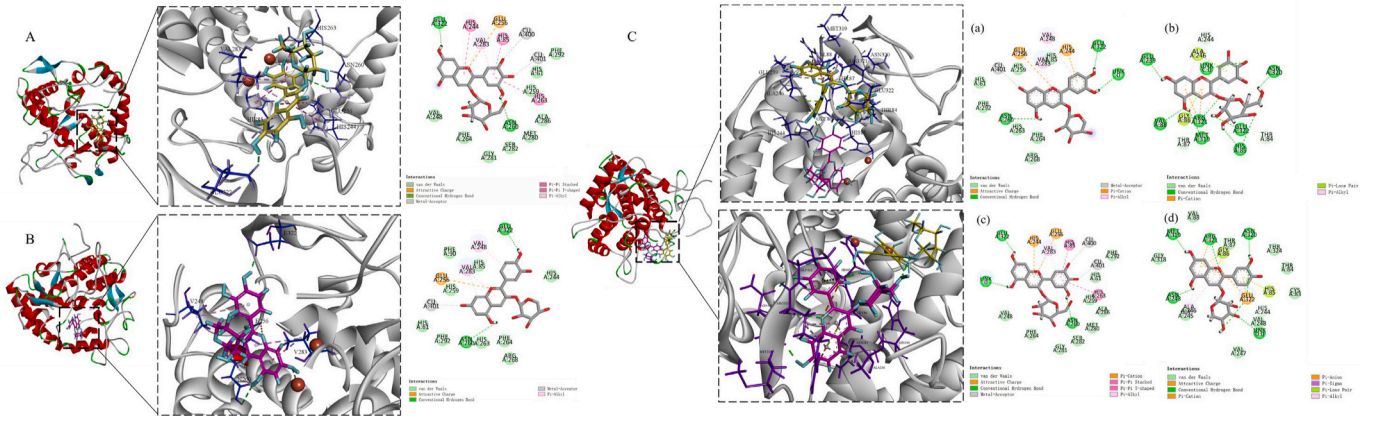

Fig. 5. Schematic diagram of TYR-D3G (A), TYR-C3A (B) and their mixture (C, TYR-C3A-D3G and TYR-D3G-C3A complex). (a–b) Tyrosinase initially docked with cyanidin-3-*O*-arabinoside followed by delphinidin-3-*O*-galactoside (c–d) Tyrosinase initially docked with delphinidin-3-*O*-galactoside followed by cyanidin-3-*O*-arabinoside. The residues were shown as balls with different colors.

Table 3
Molecular docking results of delphinidin-3-*O*-galactoside/cyanidin-3-*O*-arabinoside/ their mixture (4:1 ratio) with tyrosinase.

Complex	Donor	Residues	Distance (Å)	Types
TYR-D3G	A ring:C7-OH	Glu322	1.93	Hydrogen bond
	B ring: C3′-OH	Asn260	1.71	Hydrogen bond
	B ring, C ring	Val283	4.41, 4.81	Hydrophobic (pi-alky1)
	B ring	His85	4.12	Hydrophobic (pi-pi stacked)
	C ring	His244	5.39	Hydrophobic (pi-pi T shaped)
	B ring	His263	5.57	Hydrophobic (pi-pi T shaped)
	C ring: O	Asp312	3.4	Electrostatic (attractive charge)
	B ring: C4′-OH, C5′-OH,	Cu 401, Cu400	2.35, 2.68	Metal-Acceptor
TYR-C3A	A ring:C5-OH	Asn260	2.85	Hydrogen bond
	B ring:C4′-OH	Glu322	1.99	Hydrogen bond
	B ring	Val248	5.42	Hydrophobic (pi-alky1)
	C ring, A ring	Val283	4.86, 4.50	Hydrophobic (pi-alky1)
	C ring: O	Glu256	4.78	Electrostatic (attractive charge)
	A ring: C7-OH	Cu401	2.75	Metal-Acceptor
TYR-C3A-D3G complex	Cyanidin-3-*O*-arabinoside			
	A ring: C5-OH	Asn260	1.98, 1.96	Hydrogen bond
	B ring: C4′-OH	Glu322	1.96	Hydrogen bond
	A ring, C ring,	Val283	5.08, 5.13	Hydrophobic (pi-alky1)
	Bring	Val248	6.06	Hydrophobic (pi-alky1)
	B ring	His244	5.96	Electrostatic (pi-cation)
	C ring: O	Glu256	6.76	Electrostatic (attractive charge)
	A ring:C7-OH	Cu401	2.75	Metal-Acceptor
	Delphinidin-3-*O*-galactoside			
	Glycone: 3″, 4″	His85	1.81, 2.04	Hydrogen bond
	Glycone: 2″	Glu322	1.86	Hydrogen bond
	Glycone: 6″	Asn320	1.80	Hydrogen bond
	A ring:C5-OH	Val88, Met319	1.82, 2.41	Hydrogen bond
	A ring:C7-OH	Glu239	1.98	Hydrogen bond
	Glycone-C ring (O)	Arg321	2.20	Hydrogen bond
	A ring, C ring	Ala246	4.91, 4.79	Hydrophobic (pi-alkyl)
	B ring	Arg321	5.20	Hydrophobic (pi-alkyl)
	A ring, C ring	Arg321	3.45, 3.28	Electrostatic (pi-cation)
	B ring, C ring	Ala246, Gly86	2.86, 2.89	Pi-lone pair
	Cyanidin-3-*O*-arabinoside and Delphinidin-3-*O*-galactoside			
	B ring:C3′	B ring:C4’	2.15	Hydrogen bond
TYR-D3G-C3A complex	Delphinidin-3-*O*-galactoside			
	A ring:C7-OH	Glu322	3.68	Hydrogen bond
	B ring:C3′-OH	Asn260	2.92	Hydrogen bond
	B ring, C ring	Val283	4.43, 4.82	Hydrophobic (pi-alky1)
	B ring	His85	4.29	Hydrophobic (pi-pi stacked)
	B ring	His263	7.58	Hydrophobic (pi-pi T shaped)
	C ring: O	Glu256	7.98	Electrostatic (attractive charge)
	B ring: C4′-OH, C5′-OH,	Cu 401, Cu400	2.68, 2.39	Metal-Acceptor
	Cyanidin-3-*O*-arabinoside			
	A ring: C5-OH,	Asn243	3.76	Hydrogen bond
	A ring: C7-OH	Met319	3.88	Hydrogen bond
	B ring: C3’-OH	Asn320	3.90	Hydrogen bond
	C ring: O	Arg321	3.76	Hydrogen bond
	B ring: C3′-OH, Glycone: 4″	Glu322	3.75, 4.42	Hydrogen bond
	A ring, C ring	Ala246	3.90, 5.68	Hydrophobic (pi-alky1)
	C ring	Arg321	3.76	Hydrophobic (pi-alky1)
	B ring	Glu322	3.75	Hydrophobic (pi-sigma)
	C ring: O	Glu322	5.03	Electrostatic (attractive charge)
	B ring	Glu322	3.75	Electrostatic (pi-anion)
	A ring	Arg321	4.58	Electrostatic (pi-cation)
	A ring, C ring	Gly86	4.31, 4.87	Pi-lone pair
	B ring	His85	6.44	Pi-lone pair
	Delphinidin-3-*O*-galactoside and cyanidin-3-*O*-arabinoside			
	A ring: 5-OH,	Glycone: 3″	7.97	Hydrogen bond

TYR-C3A-D3G complex has the lowest average RMSD (0.19 ± 0.01 nm) value among the four complexes. Rg as a physical quantity describing the compactness of protein structure, can reveal the stability of the overall protein structure before and after ligand binding. The Rg values of the four complexes ranged from 2.06 to 2.08 nm, whereas TYR-C3A-D3G complex (2.07 nm) exhibited the smallest value. SASA provides the degree of information change in the binding process by analyzing the effect of ligand binding on TYR solvent accessibility. The SASA fluctuation magnitudes were 15.92 nm^2 (TYR-D3G), 18.74 nm^2 (TYR-C3A), 15.91 nm^2 (TYR-C3A-D3G), and 16.65 nm^2 (TYR-D3G-C3A), indicating that TYR-C3A-D3G complex exhibited the smallest perturbation in residue microenvironment. RMSF describes how individual atoms or residues change over time with respect to their initial structural positions. Four systems exhibited similar RMSF trends, with heightened flexibility in residues 60–80 and 239–258. Notably, TYR-C3A-D3G complex showed minimal RMSF fluctuations (residues 239–258), indicating suppressed dynamics in this flexible region. Hydrogen bonding, as a strong noncovalent interaction, facilitates ligand recognition and binding to active sites, the number of hydrogen bonds of TYR-C3A-D3G complex was the most (8). Therefore, RMSD, Rg, SASA, RMSF, and hydrogen bonds analyses demonstrated that TYR-C3A-D3G exhibited the highest structural stability among the four systems.

As Fig. 6F–I showed, MM/PBSA binding free energy decomposition analysis identified the following residues as the primary contributors to binding: His85 (−2.443 kcal/mol) for TYR-D3G, His259 (−3.118 kcal/mol) for TYR-C3A, His85 (−4.899 kcal/mol) for TYR-C3A-D3G, and Asn320 (−3.901 kcal/mol) for TYR-D3G-C3A, respectively. Fig. 6J–M illustrated that TYR-C3A-D3G displayed the strongest total binding free energy (−87.97 kcal/mol), indicating the highest affinity. The binding was dominated by favorable contributions from van der Waals energy (−84.78 kcal/mol), electrostatic energy (−120.52 kcal/mol) and nonpolar solvation energy (−13.97 kcal/mol) (where negative values indicate favorable interactions, and vice versa). As shown in Fig. 6N–Q, Gibbs free energy spectra provided insight into the conformational behavior of protein-ligand interactions. TYR-C3A-D3G complex displayed the deepest free energy valley, forming a single energy cluster, and exhibited the smallest conformation shift on the free energy potential surface. As a result, the TYR-C3A-D3G complex induced a conformational change that made the structure more compact. This

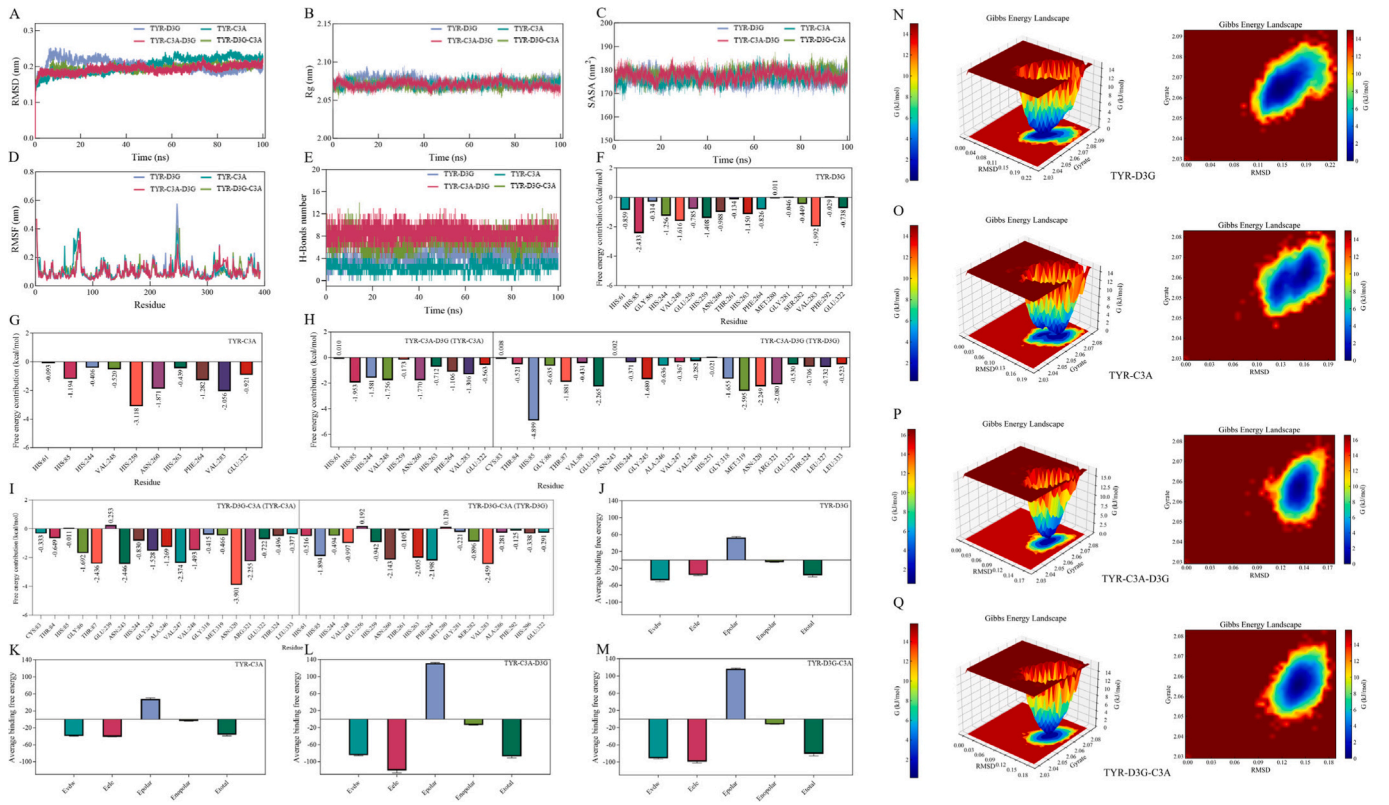

Fig. 6. The interaction of receptor tyrosinase and delphinidin-3-*O*-galactoside, cyanidin-3-*O*-arabinoside and their mixture during molecular dynamics simulation. (A) RMSD; (B) Rg; (C) SASA; (D) RMSF; (E) The number of hydrogen bonds; (F–I) Binding free energy of key amino acid residues via Gmx_MMPBSA method; (J–M) Average binding free energy of complexes; (N-Q) Gibbs free energy landscape of complex.

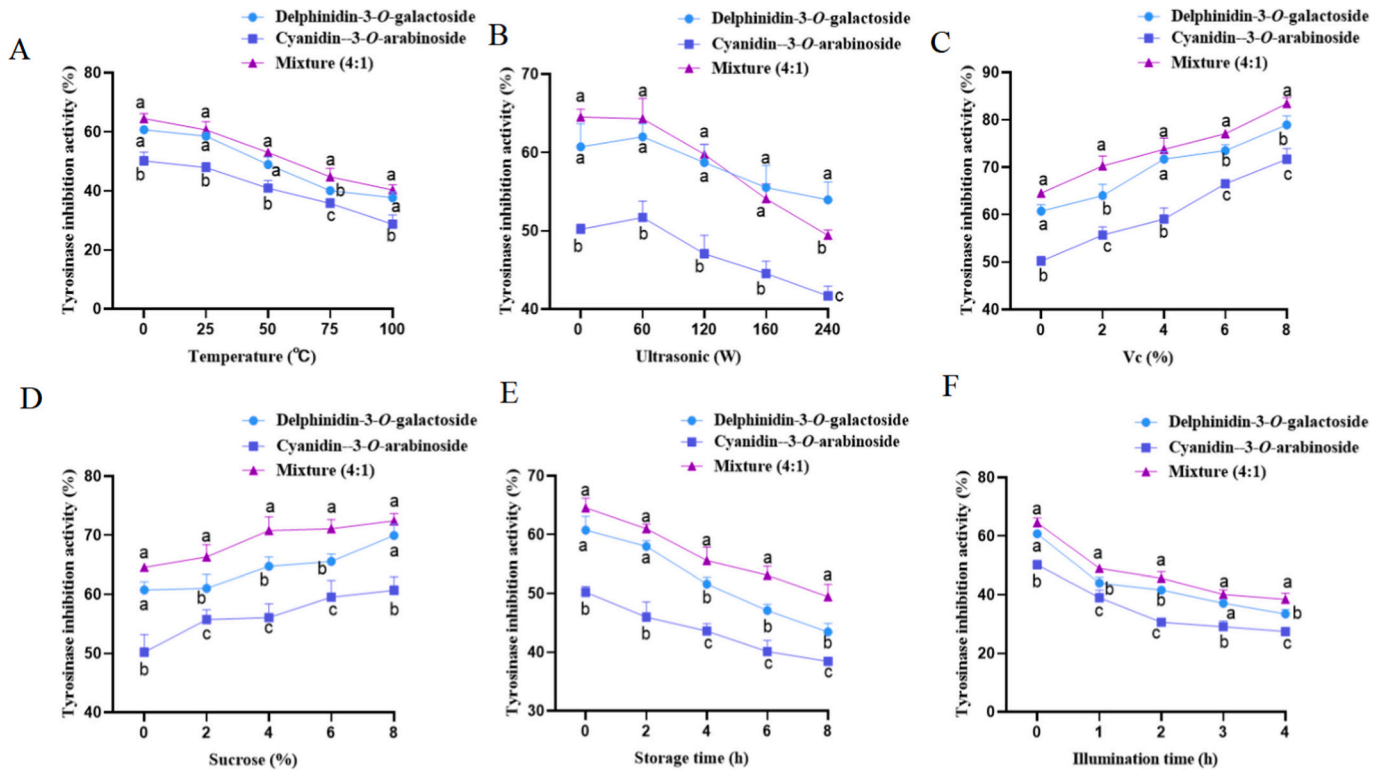

Fig. 7. Inhibition rates of tyrosinase activity of delphinidin-3-*O*-galactoside, cyanidin-3-*O*-arabinoside, and their mixture (4:1 ratio) at (A–F) different processing methods (thermal and ultrasonication), storage conditions (illumination and over storage) and additives (vitamin C and sucrose). Different letters indicate significant differences in delphinidin-3-*O*-galactoside, cyanidin-3-*O*-arabinoside, and their mixture treatment groups ($p < 0.05$).

structural change also limited substrate access to the active site, thereby inhibiting the enzyme's activity. Thus, our work not only confirms the presence of synergy but, more importantly, unveils the underlying ordered-binding mechanism.

3.8. Effect of simulated processing treatments on synergistic activity

During food manufacturing and storage, multiple factors include thermal/nonthermal processing, exposure to light and the use of additives such as sucrose and vitamins, can impact on the quality and function of processed food (Zang et al., 2022). Therefore, an investigation was conducted regarding the tyrosinase inhibition activity of delphinidin-3-*O*-galactoside/cyanidin-3-*O*-arabinoside and their mixture (4:1 ratio). The aim was to assess the impact of simulated processing treatments on their synergistic activity. The implementation of treatments such as thermal processing, ultrasonication, and specific storage conditions resulted in a decline in the inhibition rate of tyrosinase activity. At a temperature of 75 °C, the mixture (4:1 ratio) displayed a higher inhibitory activity of 44.76% ± 2.83% in comparison with the individual compounds. When the ultrasonic conditions were set under the 60 W, the mixture (4:1 ratio) demonstrated a higher tyrosinase inhibition activity of 64.3% ± 2.57% compared with that of cyanidin-3-*O*-arabinoside. However, upon increasing the ultrasonic condition to 160 W, the inhibitory rate of the mixture (4:1 ratio) on tyrosinase was lower than that of delphinidin-3-*O*-galactoside, indicating that excessive ultrasound power may disrupt the interaction between anthocyanins, leading to a weakened synergistic effect (Fig. 7A–B). The tyrosinase inhibition rates increased with increasing concentrations of Vc and sucrose. This can be ascribed to the intrinsic high antioxidant property of Vc and the formation of co-complex with sucrose, contributing to the uptrends trend of tyrosinase inhibitory activity (Li et al., 2019; Miao et al., 2019). The anthocyanin mixture exhibited a higher tyrosinase inhibition activity, with a significant difference in tyrosinase inhibition rates being observed when adding 2%, 6% and 8% of Vc and 2%–4% of sucrose was added (Fig. 7C–D). The tyrosinase inhibition rate under different storage durations and illumination times are shown in Fig. 7E–F. A significant difference in the tyrosinase inhibition rates was observed when stored for 4–8 h and exposed to light for 1, 2, and 4 h.

These results indicated that under various simulated processing conditions, including temperature, ultrasound-assisted processing, food additives and storage, the mixture (4:1 ratio) maintained a significantly higher tyrosinase inhibition rate compared to delphinidin-3-*O*-galactoside or cyanidin-3-*O*-arabinoside alone. The robustness observed under simulated conditions indicates promising adaptability in common processing conditions. Future validation in complex food matrices and cell-based systems is needed to confirm compatibility, efficacy, and biological relevance. Thus, this work not only presents effective formulation but also demonstrates a generalizable paradigm that shifts product development from empirical to mechanism-based rational design.

4. Conclusion

In summary, this study demonstrated a robust synergistic effect of blueberry and black chokeberry extract on tyrosinase inhibition activity, with an optimal molar ratio of 1:1. Using AUF–UPLC–MS/MS, sixteen tyrosinase inhibitors were screened and identified from these extracts. Among these, the primary active ingredients delphinidin-3-*O*-galactoside and cyanidin-3-*O*-arabinoside exhibited strong synergistic inhibition at 4:1 ratio and acted as mixed-type inhibitors. Compared to the individual compounds, the mixture induced enhanced intrinsic fluorescence quenching and greater alterations in the secondary conformation of tyrosinase. Molecular docking and dynamics simulations revealed that the mixture binds more stably to the enzyme's active site, facilitated by increased hydrogen bonding and hydrophobic interactions, particularly within the TYR-C3A-D3G complex. Activity verification further showed that the mixture maintained significantly higher inhibition under simulated processing conditions compared to its individual components. This research provided novel insights into the synergistic mechanisms of berry extracts and promoted the efficient development of functional foods utilizing berry-derived tyrosinase inhibitors.

CRediT authorship contribution statement

Yuxin Du: Writing – original draft, Validation, Methodology, Data curation. **Lanqiong Zhao:** Writing – original draft, Software, Methodology, Data curation. **Zixuan Yuan:** Writing – review & editing. **Yu Zhang:** Validation, Methodology. **Yuxin Chen:** Writing – review & editing. **Yang Ding:** Writing – review & editing. **Xinyao Jiao:** Validation, Resources. **Chong Zhao:** Conceptualization. **Kuniyoshi Shimizu:** Supervision. **Baoru Yang:** Resources. **Zhongxia Li:** Funding acquisition. **Bin Li:** Supervision, Resources. **Hui Tan:** Writing – review & editing, Validation, Supervision, Methodology, Conceptualization.

Declaration of competing interest

The authors declare that they have no known competing financial interests or personal relationships that could have appeared to influence the work reported in this paper.

Acknowledgments

This manuscript was supported by “By-Health Nutrition Research Grant (TY202101071)”, China Green Food Development Center Grant (GF-TSPZ-2024004-1)” and “the Young Scientists Fund of the National Natural Science Foundation of China (32502265)”.

Appendix A. Supplementary data

Supplementary data to this article can be found online at https://doi.org/10.1016/j.fochx.2025.103464.

Data availability

Data will be made available on request.

References

Abdurrahim, A. E., Temelli, F., Mazurak, V., Benruwin, R. A., & Chen, L. (2021). Anthocyanin and gingerol extracts exhibit a synergistic effect to inhibit the proliferation of Caco-2, Hep G2, and HT-29 cells *in vitro*. *ACS Food Science & Technology, 1*, 1642–1651. https://doi.org/10.1021/acsfoodscitech.1c00029

Aramwit, P., Bang, N., & Srichana, T. (2010). The properties and stability of anthocyanins in mulberry fruits. *Food Research International, 43*, 1093–1097. https://doi.org/10.1016/j.foodres.2010.01.022

Caksa, S., Baqai, U., & Aplin, A. E. (2022). The future of targeted kinase inhibitors in melanoma. *Pharmacology & Therapeutics, 239*, Article 108200. https://doi.org/10.1016/j.pharmthera.2022.108200

Cardullo, N., Muccilli, V., Pulvirenti, L., Cornu, A., Pouységu, L., Deffieux, D., … Tringali, C. (2020). C-glucosidic ellagitannins and galloylated glucoses as potential functional food ingredients with anti-diabetic properties: A study of α-glucosidase and α-amylase inhibition. *Food Chemistry, 313*, Article 126099. https://doi.org/10.1016/j.foodchem.2019.126099

Chou, T. C., Shapiro, T. A., Fu, J., Chou, J. H., & Ulrich-Merzenich, G. S. (2019). Computerized quantification of drugs synergism in animal studies or in clinical trials using only ten data points. *Synergy, 9*, Article 100049. https://doi.org/10.1016/J.SYNRES.2019.100049

Copeland, R. A. (2013). Evaluation of enzyme inhibitors in drug discovery: A guide for medicinal chemists and pharmacologists. In R. A. Copeland (Ed.), *Reversible modes of inhibitor interactions with enzymes* (pp. 281–304). John Wiley & Sons Inc.

Decker, H., & Tuczek, F. (2017). The recent crystal structure of human tyrosinase related protein 1 (HsTYRP1) solves an old problem and poses a new one. *Angewandte Chemie International Edition, 56*, 14352–14354. https://doi.org/10.1002/anie.201708214

Gao, N., Si, X., Han, W., Gong, E., Shu, C., Tian, J., Wang, Y., Zhang, J., Li, B., & Li, B. (2023). The contribution of different polyphenol compositions from chokeberry produced in China to cellular antioxidant and antiproliferative activities. *Food Science and Human Wellness, 12*, 1590–1600. https://doi.org/10.1016/j.fshw.2023.02.018

Hering, A., Stefanowicz-Hajduk, J., Dziomba, S., Halasa, R., Krzemieniecki, R., Sappati, S., … Fu, Y. J. (2023). Identification of pancreatic lipase inhibitors from *Eucommia ulmoides* tea by affinity-ultrafiltration combined UPLC-Orbitrap MS and in vitro validation. *Food Chemistry, 426*, Article 136630. https://doi.org/10.1016/j.foodchem.2023.136630

Kausar, H., Jeyabalan, J., Aqil, F., Chabba, D., Sidana, J., Singh, I. P., & Gupta, R. C. (2012). Berry anthocyanidins synergistically suppress growth and invasive potential of human non-small-cell lung cancer cells. *Cancer Letters, 325*, 54–62. https://doi.org/10.1016/j.canlet.2012.05.029

Leporini, M., Tundis, R., Sicari, V., Pellicanò, T. M., Dugay, A., Deguin, B., & Loizzo, M. R. (2020). Impact of extraction processes on phytochemicals content and biological activity of *Citrus* × *Clementina* Hort. Ex Tan. Leaves: New opportunity for under-utilized food by-products. *Food Research International, 127*, Article 108742. https://doi.org/10.1016/j.foodres.2019.108742

Li, D., Zhang, X. C., Xu, Y. Q., Li, L., Aghdam, M. S., & Luo, Z. S. (2019). Effect of exogenous sucrose on anthocyanin synthesis in postharvest strawberry fruit. *Food Chemistry, 289*, 112–120. https://doi.org/10.1016/j.foodchem.2019.03.042

Li, J., Feng, L., Liu, L., Wang, F., Ouyang, L., Zhang, L., … Wang, G. (2021). Recent advances in the design and discovery of synthetic tyrosinase inhibitor. *European Journal of Medicinal Chemistry, 224*, Article 113744. https://doi.org/10.1016/j.ejmech.2021.113744

Li, J., Yang, G. Y., Shi, W. F., Fang, X. P., Han, L. T., & Cao, Y. (2022). Anti-Alzheimer's disease active components screened out and identified from *Hedyotis diffusa* combining bioaffinity ultrafiltration LC-MS with acetylcholinesterase. *Journal of Ethnopharmacology, 296*, Article 115460. https://doi.org/10.1016/j.jep.2022.115460

Liu, Y. Y., Hu, X., Li, E., Fang, Y. J., Xue, H., Zhang, J. C., … Wang, R. (2024). Bioaffinity ultrafiltration combined with UPLC-ESI-QTrap-MS/MS for screening of xanthine oxidase inhibitors from *Paederia foetida* L. leaves. *Arabian Journal of Chemistry, 17*(4), Article 105706. https://doi.org/10.1016/j.arabjc.2024.105706

Miao, F., Su, M. Y., Jiang, S., Luo, L. F., Shi, Y., & Lei, T. C. (2019). Intramelanocytic acidification plays a role in the Antimelanogenic and Antioxidative properties of vitamin C and its derivatives. *Oxidative Medicine and Cellular Longevity, 14*, Article 2084805. https://doi.org/10.1155/2019/2084805

Molina, P. G., Saura-Sanmartin, A., Berna, J., Teruel, J. A., Muñoz Muñoz, J. L., Rodríguez López, J. N., … Molina, F. G. (2024). Considerations about the inhibition of monophenolase and diphenolase activities of tyrosinase. Characterization of the inhibitor concentration which generates 50% of inhibition, type and inhibition constants. *International Journal of Biological Macromolecules, 267*, Article 131513. https://doi.org/10.1016/j.ijbiomac.2024.131513

Muñoz-Pina, S., Duch-Calabuig, A., Ros-Lis, J., Verdejo, B., García-España, E., Argüelles, Á., & Andrés, A. (2021). A tetraazahydroxypyridinone derivative as inhibitor of apple juice enzymatic browning and oxidation. *LWT - Food Science and Technology, 154*, Article 112778. https://doi.org/10.1016/j.lwt.2021.112778

Najjar, R. S., Knapp, D., Wanders, D., & Feresin, R. G. (2022). Raspberry and blackberry act in a synergistic manner to improve cardiac redox proteins and reduce NF-kB and SAPK/JNK in mice fed a high-fat, high-sucrose diet. *Nutrition, Metabolism & Cardiovascular Diseases, 32*, 1784e1796. https://doi.org/10.1016/j.numecd.2022.03.015

Ou, R., Lin, L., Zhao, M., & Xie, Z. (2020). Action mechanisms and interaction of two key xanthine oxidase inhibitors in galangal: Combination of in vitro and in silico molecular docking studies. *International Journal of Biological Macromolecules, 162*, 1526–1535. https://doi.org/10.1016/j.ijbiomac.2020.07.297

Puiggròs, F., Muguerza, B., Arola-Arnal, A., Aragonès, G., Suárez-Garcia, S., Bladé, C., … Suárez, M. (2017). Functional beverages. In I. Aguiló-Aguayo, & L. Plaza (Eds.), *Innovative technologies in beverage processing* (pp. 275–296). Chichester UK: Wiley.

Qi, Q. Q., Chu, M. J., Yu, X. T., Xie, Y. N., Li, Y. L., Du, Y. M., … Yan, N. (2023). Anthocyanins and proanthocyanidins: Chemical structures, food sources, bioactivities, and product development. *Food Reviews International, 39*, 4581–4609. https://doi.org/10.1080/87559129.2022.2029479

Song, X., Hu, X., Zhang, Y., Pan, J., Gong, D., & Zhang, G. (2020). Inhibitory mechanism of epicatechin gallate on tyrosinase: Inhibitory interaction, conformational change and computational simulation. *Food & Function, 11*, 4892–4902. https://doi.org/10.1039/d0fo00003e

Song, X., Ni, M., Zhang, Y., Zhang, G., Pan, J., & Gong, D. (2021). Comparing the inhibitory abilities of epigallocatechin-3-gallate and gallocatechin gallate against tyrosinase and their combined effects with kojic acid. *Food Chemistry, 349*, Article 129172. https://doi.org/10.1016/j.foodchem.2021.129172

Tan, H., Cui, B. Y., Zheng, K. X., Gao, N. X., An, X. N., Zhang, Y., Cheng, Z., Nie, Y. J., Zhu, J. Y., Wang, L., Shimizu, K., Sun, X. Y., & Li, B. (2024). Novel inhibitory effect of black chokeberry (*Aronia melanocarpa*) from selected eight berries extracts on advanced glycation end-products formation and corresponding mechanism study. *Food Chemistry: X, 21*, Article 101032. https://doi.org/10.1016/j.fochx.2023.101032

Theba, T., Nayi, P., & Ravani, A. (2024). Beetroot-based blended juice: Process development, physicochemical analysis and optimization of novel health drink. *Food Chemistry Advances, 4*, Article 100607. https://doi.org/10.1016/j.focha.2024.100607

Tian, S., Li, X., Zang, S., Jin, Y., Zhang, Z., & Yu, Y. (2021). α-Amylase and tyrosinase inhibitory activities, phenolic contents, and antioxidant capacities of wild and cultivated blueberries. *Journal of Food Processing and Preservation, 45*, Article e15087. https://doi.org/10.1111/jfpp.15087

Wang, R., Wang, G. H., Xia, Y., Sui, W. J., & Si, C. L. (2019). Functionality study of lignin as a tyrosinase inhibitor: Influence of lignin heterogeneity on anti-tyrosinase activity. *International Journal of Biological Macromolecules, 128*, 107–113. https://doi.org/10.1016/j.ijbiomac.2019.01.089

Wazed, M. A., Sheikh, M. M. A., Akhtaruzzaman, M., Awal, M. S., & Mozumder, N. H. M. R. (2023). Quality evaluation and shelf-life analysis of fruit juice cocktail containing mango (*Mangifera indica*) and pineapple (*Ananas comosus*). *Journal of Agriculture and Food Research, 14*, Article 100773. https://doi.org/10.1016/j.jafr.2023.100773

Xue, Q., Liu, X., Russell, P., Li, J., Pan, W. X., Fu, J. J., & Zhang, A. Q. (2022). Evaluation of the binding performance of flavonoids to estrogen receptor alpha by Autodock, Autodock Vina and Surflex-Dock. *Ecotoxicology and Environmental Safety, 233*, Article 113323. https://doi.org/10.1016/j.ecoenv.2022.113323

Zang, Z. H., Chou, S. R., Geng, L. R., Si, X., Ding, Y. M., Lang, Y. X., … Tian, J. L. (2021). Interactions of blueberry anthocyanins with whey protein isolate and bovine serum protein: Color stability, antioxidant activity, *in vitro* simulation, and protein functionality. *LWT - Food Science and Technology, 152*, Article 112269. https://doi.org/10.1016/j.lwt.2021.112269

Zang, Z. H., Chou, S. R., Si, X., Cui, H. J., Tan, H., Ding, Y. M., … Tian, J. L. (2022). Effect of bovine serum albumin on the stability and antioxidant activity of blueberry anthocyanins during processing and in vitro simulated digestion. *Food Chemistry, 373*, Article 131496. https://doi.org/10.1016/j.foodchem.2021.131496

Zhang, C., Zhang, B., Zhang, L., Adel Ashour, A., Wang, Y., Zhang, Y., … Jiao, X. (2024). Malvidin-3-*O*-galactoside ameliorates colonic mucosal barrier function via the notch signaling pathway. *Food Innovation and Advances, 3*(3), 279–287. https://doi.org/10.48130/fia-0024-0026

Zhang, L. L., Guan, Q. H., Tang, L. H., Jiang, J. C., Sun, K., Manirafasha, E., & Zhang, M. (2023). Effect of Cu^{2+} and Al^{3+} on the interaction of chlorogenic acid and caffeic acid with serum albumin. *Food Chemistry, 410*, Article 135406. https://doi.org/10.1016/j.foodchem.2023.135406

Zhao, L., Wen, L., Lu, Q., & Liu, R. (2020). Interaction mechanism between α-glucosidase and A-type trimer procyanidin revealed by integrated spectroscopic analysis techniques. *International Journal of Biological Macromolecules, 143*, 173–180. https://doi.org/10.1016/j.ijbiomac.2019.12.021

Zhu, J., Chen, X., Luo, J. W., Liu, Y. J., Wang, B., Liang, Z. L., & Lin, L. (2021). Insight into the binding modes and mechanisms of inhibition between soybean-peptides and α-amylase based on spectrofluorimetry and kinetic analysis. *LWT - Food Science and Technology, 142*, Article 110977. https://doi.org/10.1016/j.lwt.2021.110977

Zhu, Y., Ling, W., Guo, H., Song, F., Ye, Q., Zou, T., Li, D., Zhang, Y., Li, G., Xiao, Y., Liu, F., Li, Z., Shi, Z., & Yang, Y. (2013). Anti-inflammatory effect of purified dietary anthocyanin in adults with hypercholesterolemia: A randomized controlled trial. *Nutrition, Metabolism & Cardiovascular Diseases, 23*, 843–849. https://doi.org/10.1016/j.numecd.2012.06.005

Zolghadri, S., Bahrami, A., Hassan Khan, M. T., Munoz-Munoz, J., Garcia-Molina, F., Garcia-Canovas, F., & Saboury, A. A. (2019). A comprehensive review on tyrosinase inhibitors. *Journal of Enzyme Inhibition and Medicinal Chemistry, 34*, 279–309. https://doi.org/10.1080/14756366.2018.1545767